Muon spin rotation and relaxation in $Pr_{1-x}Nd_xOs_4Sb_{12}$: Superconductivity and magnetism in Pr-rich alloys

P.-C. Ho [ORCID],[1] D. E. MacLaughlin,[2] M. B. Maple,[3] Lei Shu,[4,5] A. D. Hillier,[6] O. O. Bernal [ORCID],[7] T. Yanagisawa [ORCID],[8]
P. K. Biswas,[6] Jian Zhang,[4] Cheng Tan,[4] S. D. Hishida [ORCID],[1] and T. McCullough-Hunter[1]

[1]*Department of Physics, California State University, Fresno, California 93740, USA*
[2]*Department of Physics and Astronomy, University of California, Riverside, California 92521, USA*
[3]*Department of Physics, University of California, San Diego, La Jolla, California 92093, USA*
[4]*State Key Laboratory of Surface Physics and Department of Physics, Fudan University, Shanghai 200438, China*
[5]*Shanghai Research Center for Quantum Sciences, Shanghai 201315, China*
[6]*ISIS Facility, Rutherford Appleton Laboratory, Chilton, Didcot Oxon OX11 0QX, United Kingdom*
[7]*Department of Physics and Astronomy, California State University, Los Angeles, California 90032, USA*
[8]*Department of Physics, Hokkaido University, Sapporo, Hokkaido 060-0810, Japan*

The Pr-rich end $0 \leqslant x \leqslant 0.25$ of the alloy series $Pr_{1-x}Nd_xOs_4Sb_{12}$ has been studied using muon spin rotation and relaxation. The end compound $PrOs_4Sb_{12}$ is an unconventional heavy-fermion superconductor, which exhibits a spontaneous magnetic field associated with broken time-reversal symmetry (TRS) in the superconducting phase. No such field is observed in the Nd-doped alloys for $x \geqslant 0.05$, indicating that TRS has been restored. The superfluid density from the vortex-lattice field distribution is insensitive to Nd concentration for $x \lesssim 0.2$, indicating that TRS restoration does not have a strong effect on the superconducting state. No Nd^{3+} static magnetism, ordered or disordered, is found down to the lowest temperatures of measurement.

I. INTRODUCTION

Unconventional superconductivity was discovered in the filled skutterudite compound $PrOs_4Sb_{12}$ ($T_c = 1.85$ K) almost 20 years ago [1], but there are still many intriguing aspects of this compound that are not well understood. Two of these are the origin of its enhanced electron mass in the absence of the magnetic crystalline-electric-field ground state that is usual for heavy-fermion compounds [2,3], and the mechanism or mechanisms responsible for its multiple superconducting phases; the superconducting gap symmetry, in particular, is controversial [4–9]. An internal magnetic field was detected via muon spin relaxation (μSR) [10] in the zero-field (ZF) superconducting state [11], indicative of broken time reversal symmetry (TRS) [12]. The appearance of superconductivity in $PrOs_4Sb_{12}$ is close to an antiferroquadrupolar phase for magnetic fields H between 4.5 T and 14.5 T [13,14], raising the possibility that the pairing mechanism involves quadrupolar [15–18] or higher-order multipolar [19] fluctuations.

Other rare-earth filled-skutterudite compounds order magnetically at quite low temperatures: spin-density-wave type antiferromagnetism in $CeOs_4Sb_{12}$ occurs below 1 K [20–23], weak ferromagnetism in $SmOs_4Sb_{12}$ develops below 2.6 K [24], and ferromagnetism in $NdOs_4Sb_{12}$ appears below 1 K [25]. The latter led to speculation that the origin of the superconducting pairing mechanism in $PrOs_4Sb_{12}$ could be quantum fluctuations near a magnetic quantum critical point.

The $Pr_{1-x}Nd_xOs_4Sb_{12}$ substitutional alloy system has been studied [26–28] to investigate the interplay between ferromagnetism and the unconventional superconductivity in $PrOs_4Sb_{12}$. The phase diagram of the superconducting and ferromagnetic transition temperatures (T_c and T_{Curie}, respectively) versus Nd concentration x is shown in Fig. 1 [28,29], together with the onset of broken TRS at T_c for $x = 0$ [11,30,31]. One of the major features is the relative insensitivity of T_c to Nd doping; the rate of decrease is comparable to that for nonmagnetic Ru doping [27] and much slower than for rare-earth doping of both conventional and unconventional superconductors. The initial slope $(dT_c/dx)_0/T_c$ is $-0.012/\%$ in $Pr_{1-x}Nd_xOs_4Sb_{12}$, compared to, for example, $-0.94/\%$ in $La_{1-x}Gd_xIn_3$ [32] and $\sim-0.30/\%$ in heavy-fermion $U_{1-x}R_xBe_{13}$, $R =$ La, Gd, Lu, and Th [33].

This paper reports results of a study of Pr-rich $Pr_{1-x}Nd_xOs_4Sb_{12}$, $x = 0$, 0.05, 0.10, 0.15, 0.20, and 0.25, using ZF and transverse-field (TF) [34] μSR. With ZF μSR we observe the onset at $T = T_c$ of the previously reported spontaneous internal field for $x = 0$ [11,31], but for $x = 0.05$ and higher no such field is observed down to the lowest temperatures of measurement. This is a surprising result, since rapid restoration of TRS by magnetic moments seems peculiar when ordered magnetism breaks TRS. The $T=0$ superfluid density $\rho_s(0)$ measured using TF μSR is remarkably independent of x for $x \leqslant 0.2$, suggesting only a small difference, if any, between the broken-TRS ($x = 0$) and restored-TRS superconducting states. For $x \gtrsim 0.1$, the dynamic muon relaxation rate increases with decreasing temperature down to

the lowest temperatures of measurement. This is reminiscent of critical slowing at a magnetic phase transition, but no magnetic transition is observed for $x \leqslant 0.25$ down to the lowest temperatures of measurement.

II. EXPERIMENT

Single crystals of $Pr_{1-x}Nd_xOs_4Sb_{12}$, $x = 0.05$, 0.10, 0.15, and 0.20, were prepared by the antimony self-flux growth method [20]. Praseodymium and neodymium were premixed using a single-arc furnace. X-ray powder diffraction measurements were made to confirm the alloys have the cubic $LaFe_4P_{12}$-type structure [35]. For each concentration, $\sim$2-g clusters of single crystals were attached to silver sample holders using GE-7031 varnish.

Positive-muon (μ^+) μSR experiments were carried out using dilution refrigerators at the ISIS muon facility, STFC Rutherford Appleton Laboratory, UK, over the temperature range 0.025–3 K, in ZF and TF (field perpendicular to the initial μ^+ spin polarization) between 0 and 200 Oe. For the ZF μSR experiments, the field was zeroed to within $\sim$1 μT. Data were analyzed using the μSR software package MUS-RFIT [36]. Observation of temperature-dependent relaxation rates down to $\sim$100 mK is evidence for good thermalization of the samples to this temperature. Previously reported data for $x = 0$ [9,31] and 0.25 [29], obtained at ISIS and TRIUMF, Vancouver, Canada, have been reanalyzed and included here.

A brief summary of the μSR data analysis used in the present paper is given in the Appendix.

III. RESULTS

A. Zero field

Representative ZF μSR spin-polarization functions from asymmetry measurements in $Pr_{1-x}Nd_xOs_4Sb_{12}$ are shown in Fig. 2. As described in the Appendix, a silver background signal from the cryostat cold finger has been subtracted, and the sample signal has been normalized to give the polarization function $G(t)$.

It is not easy to differentiate between dynamic exponential damping and an exponential contribution to static relaxation if only early-time data are available. If, however, the data extend to late enough times, the difference in asymptotic behavior can provide a clear determination. Quite generally, $G(t \to \infty) \to 1/3$ for static ZF relaxation due to randomly oriented local fields [37] (cf. Appendix Sec. A 1), whereas $G(t \to \infty) \to 0$ for dynamic relaxation.

The solid curves in Fig. 2 are fits to the data of the exponentially damped Gaussian Kubo-Toyabe (KT) function [37]:

$$G(t) = e^{-\lambda_d t}\left\{\frac{1}{3} + \frac{2}{3}\left[1 - (\Delta_{KT}t)^2\right]\exp\left[-\frac{1}{2}(\Delta_{KT}t)^2\right]\right\} \quad (1)$$

(cf. Appendix Sec. A 1). This models the combined effect of dynamically fluctuating local fields (relaxation rate λ_d) and a Gaussian distribution of randomly oriented static fields with rms width Δ_{KT}/γ_μ; here $\gamma_\mu = 8.5156 \times 10^8\,\text{s}^{-1}\,\text{T}^{-1}$ is the muon gyromagnetic ratio.

The dashed curves in Fig. 2 are not fits; they are the undamped ZF static Voigtian KT relaxation function $G_V(\Delta_{KT}, a, t)$ [Eq. (A5)] appropriate to a convolution of
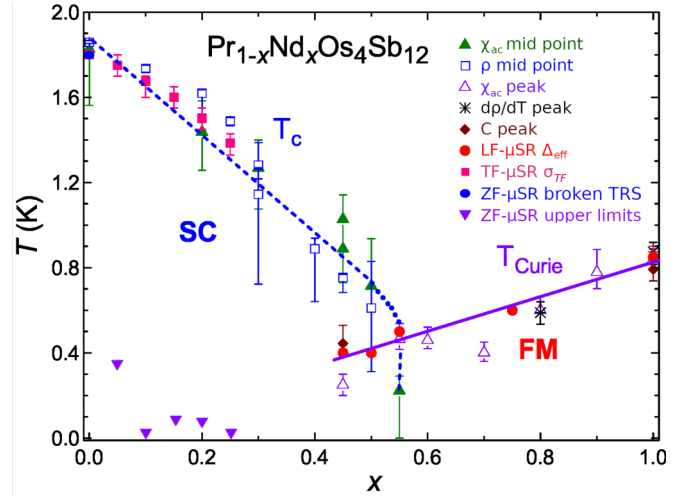

FIG. 1. Phase diagram of $Pr_{1-x}Nd_xOs_4Sb_{12}$. Superconducting and ferromagnetic transition temperatures (T_c and T_{Curie}, respectively) from electrical resistivity ρ, magnetic susceptibility χ, specific heat C [28], and μSR ([29], this paper), onset of broken TRS, $x = 0$ from ZF μSR [11,30,31], and upper temperature limits for static Nd^{3+} magnetism and/or broken TRS from ZF μSR (this paper).

purely static Gaussian and Lorentzian field distributions [38], with Gaussian rate Δ_{KT} and exponential rate a fixed at values from the damped Gaussian fits ($a = \lambda_d$). Agreement is good at early times, but the Voigtian functions exhibit the late-time approach to 1/3 characteristic of static ZF relaxation in disagreement with the experimental data. The observed decay to zero is strong evidence that the exponential relaxation is dynamic in origin. *Damped* Voigtian fits to the data [Appendix Eq. (A6) with $G_{stat}(t) = G_V(\Delta_{KT}, a, t)$, Eq. (A5)] yield $a \approx 0$ (Appendix Sec. A 1).

Figure 3 gives ZF μ^+ spin polarization functions $G(t)$ at the lowest temperatures of measurement, to show the effect of Nd doping at early times. The curves are fits of exponentially-damped static ZF Gaussian KT functions to the data as in Fig. 2. The slower relaxation for $x = 0.05$ compared to $x = 0$ is due to suppression of the spontaneous field distribution associated with broken TRS. For $x > 0.05$, the relaxation becomes faster and more nearly exponential.

The temperature and Nd concentration dependencies of the relaxation rates Δ_{KT} and λ_d are discussed in Sec. IV A.

B. Transverse field

Examples of TF μSR spin polarization functions above and below T_c for transverse field H_{TF} greater than the lower critical field H_{c1} are shown in Fig. 4 for $x = 0.05$. The silver signal has been subtracted and the sample signal has been normalized as described above and in the Appendix. The curves are fits to the data of the exponentially damped TF Gaussian relaxation function (Appendix Sec. A 2):

$$G_{TF}(t) = \exp\left[-\lambda_{TF}t - \frac{1}{2}(\sigma_{TF}t)^2\right]\cos(\omega t + \phi). \quad (A7)$$

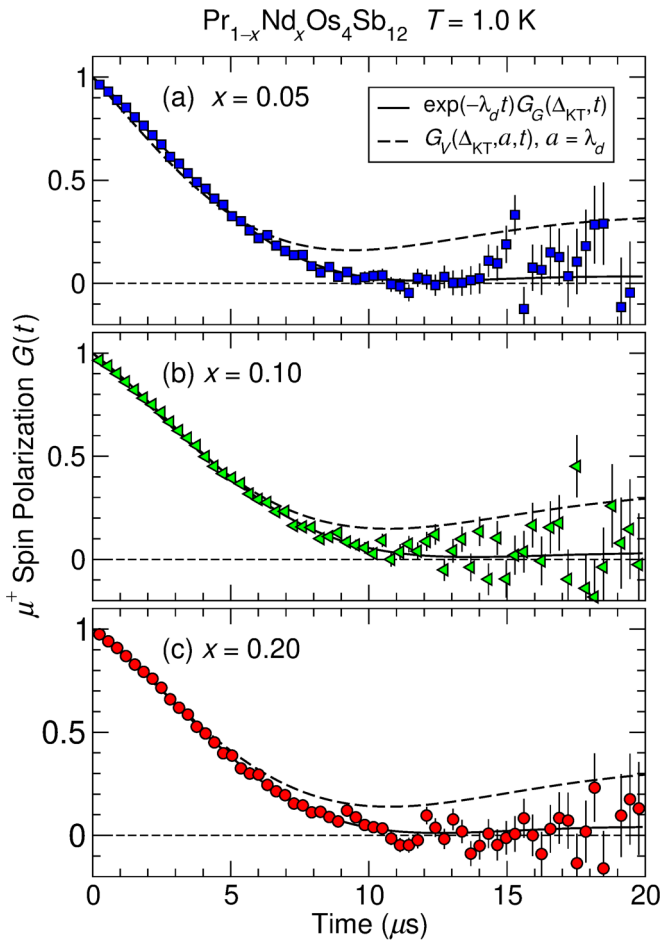The rapid damping for $T = 1.0$ K is due to the inhomogeneous magnetic field distribution in the vortex lattice.

FIG. 2. Zero-field μ^+ spin polarization $G(t)$ in $Pr_{1-x}Nd_x$ Os_4Sb_{12}, $T = 1$ K. (a) $x = 0.05$. (b) $x = 0.10$. (c) $x = 0.20$. Solid curves: Fits of exponentially damped static ZF Gaussian KT function [Eq. (1)] to the data. Dashed curves: Plots (not fits) of undamped Voigtian functions [Appendix Eq. (A5)] with Δ_{KT} and static exponential rate $a = \lambda_d$ from damped Gaussian fits (Appendix Sec. A 1).

Section IV B discusses the Nd concentration and temperature dependencies of the Gaussian and exponential relaxation rates from fits of Eq. (A7) to the data.

IV. DISCUSSION

A. Zero field

Figure 5 shows the temperature dependence of the ZF relaxation rates Δ_{KT} and λ_d from fits of Eq. (1) to the data. Data below ∼0.07 K show little temperature dependence, which is perhaps a sign of lack of thermalization at these temperatures. We concentrate on the results above ∼0.1 K.

For $x = 0$, the Gaussian static rate Δ_{KT} increases below T_c due to the spontaneous local field from broken TRS in the superconducting state [11,30,31]. When Pr is substituted with Nd, the relatively slow variation of T_c with increase of Nd concentration (Fig. 1) might have suggested a correspondingly slow suppression of broken TRS, as is found for nonmagnetic La or Ru doping [31]. In addition, magnetic-impurity-induced broken TRS has been theoretically predicted [39–41]. In
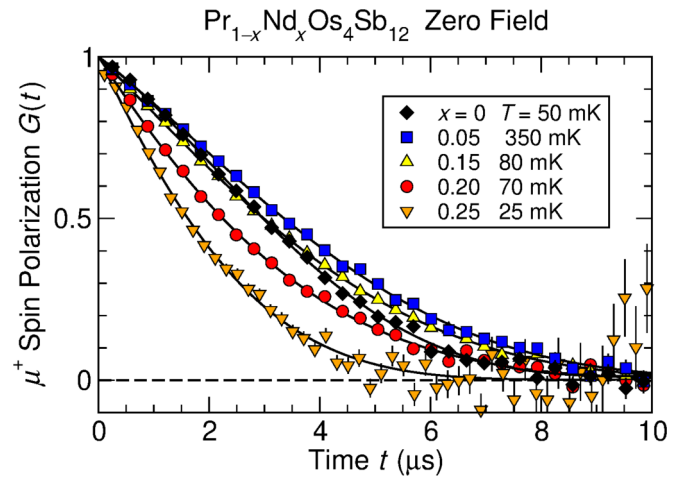

FIG. 3. Zero-field relaxation of μ^+ spin polarization $G(t)$ in $Pr_{1-x}Nd_xOs_4Sb_{12}$, $x = 0$, 0.5, 0.15, 0.20, and 0.25, at the lowest temperatures of measurement. Solid curves: Fits of exponentially damped static ZF Gaussian KT functions to the data as in Fig. 2. Results for $x = 0$ and 0.25 are from reanalysis of previously reported data (Refs. [31] and [29], respectively).

contrast, no increase of Δ_{KT} below T_c is observed for $0.05 \leqslant x \leqslant 0.20$ down to the lowest temperatures of measurement [Fig. 5(a)]. This is evidence for rapid recovery of TRS by Nd doping, and is a major result of this paper.

Broken TRS without an associated internal magnetic field is possible if there are no spontaneous defect- or surface-induced supercurrents [42] or no associated spin supercurrents [43]. It seems unlikely, however, that doping with magnetic impurities would lead to either of these situations. Thus, the observed suppression of the spontaneous field is strong evidence that TRS is restored for low Nd concentrations. To our knowledge there has been no previous observation or theory of this phenomenon.

As was previously observed for $x = 0.25$ [29], there is no oscillation or increase of Δ_{KT} at low temperatures that

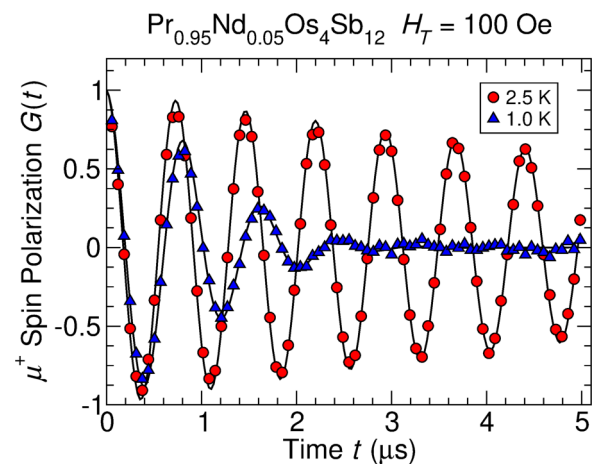FIG. 4. Time evolution of μ^+ spin polarization $G(t)$ for $Pr_{0.95}Nd_{0.05}Os_4Sb_{12}$, transverse field $H_{TF} = 100$ Oe. Circles: $T = 2.5$ K $> T_c$. Triangles: 1.0 K $< T_c$. Curves: Fits of Eq. (A7) to the data.

Pr$_{1-x}$Nd$_x$Os$_4$Sb$_{12}$ Zero Field
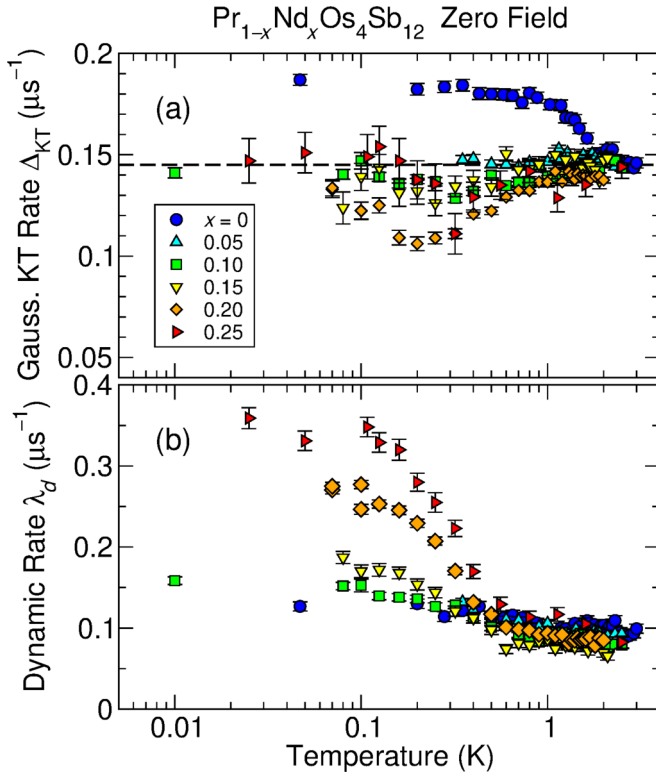

FIG. 5. Temperature dependencies of (a) static Gaussian KT rate Δ_{KT} and (b) dynamic exponential rate λ_d from fits of Eq. (1) to ZF data. Rates for $x = 0$ and $x = 0.25$ are from reanalysis of previously reported data [29,31]. Dashed line: normal-state rate for $x = 0$ from Ref. [31].

would signal the onset of static magnetism, ordered or disordered. The Gaussian rate due to μ^+ dipolar coupling to a diluted lattice of disordered Nd^{3+} static moments has been estimated [29] at $\sim 10 \, \mu s^{-1}$ for $x \sim 0.2$. This is a lower limit, since an additional RKKY-based transferred hyperfine interaction is present in the $x = 1$ end compound. The data of Fig. 5 show no such increase on a scale two orders of magnitude smaller than this estimate down to the lowest temperatures of measurement (Fig. 1). These are therefore upper bounds on both magnetic and TRS-breaking transitions.

For $x = 0$, λ_d is significant, and has been attributed to hyperfine-enhanced ^{141}Pr nuclear spin dynamics [44]. In the Nd-doped alloys, λ_d exhibits an upturn at low temperatures, the size of which increases with increasing x. This is reminiscent of critical slowing associated with a magnetic phase transition, and is evidence that Nd^{3+} spin fluctuations are involved but magnetic freezing is not present down to the lowest temperatures of measurement. This is surprising, since the paramagnetic Curie-Weiss temperature is ~ -1 K for $x = 0.2$ [28], suggesting antiferromagnetic correlations. At this concentration, the Curie constant corresponds to an effective Nd^{3+} moment $\sim 2.5 \mu_B$, which is close to the value for $x = 1$ [25]. Spin freezing might therefore have been expected not too far below 1 K. Furthermore, extrapolation of the linear ferromagnetic Curie temperature $T_{Curie}(x)$ observed for $x \geqslant 0.45$ (Fig. 1) to low Nd concentrations yields estimated transitions at experimentally attained temperatures (e.g., 0.2 K

for $x = 0.25$). As discussed in the previous paragraph, the resulting static μ^+ relaxation rate from magnetic freezing of Nd moments would be much larger than observed (Fig. 5).

It might be argued that for $x > 0$ the increase of λ_d and statistical anticorrelation between Δ_{KT} and λ_d in Eq. (1), rather than restoration of TRS, causes the absence of an increase of $\Delta_{KT}(T)$. These parameters are moderately correlated in the fits (correlation coefficients ~ -0.5), which may contribute to the decrease of $\Delta_{KT}(T)$ at low temperatures discussed below. We note, however, that for $x = 0$ the rate increase clearly begins at T_c, whereas in the Nd-doped alloys the increase of $\lambda_d(T)$ does not begin strongly until considerably below T_c. In particular, $\lambda_d(T)$ is nearly the same for $x = 0$ and $x = 0.05$, but for $x = 0.05$ Δ_{KT} is temperature independent to within errors. Thus, restoration of TRS by Nd doping is considerably more likely than an artifact of correlation.

For higher Nd concentrations, $\Delta_{KT}(T)$ decreases somewhat at intermediate temperatures. Apart from the statistical anticorrelation mentioned above, this would be expected from the spin dynamics: slowing of Nd^{3+} fluctuations increases the dynamic relaxation rate of nuclear spins as well as μ^+ spins. Then nuclear dipolar fields at μ^+ sites might no longer be quasistatic, and the μ^+ relaxation rate would be reduced [37]. The subsequent slight increase in $\Delta_{KT}(T)$ at lower temperatures is not well understood.

Presumably, the contribution to $\lambda_d(T)$ from fluctuating nuclear moments [44] is similarly motionally narrowed (decreased) by increased nuclear spin-lattice relaxation. But $\lambda_d(T)$ increases with decreasing temperature, at a rate that increases with increasing x [Fig. 5(b)]. This is strong evidence that direct relaxation by Nd^{3+} spins is dominant.

B. Transverse field

1. Gaussian rate

The distribution of the magnetic field in the vortex state is not expected to be Gaussian [45,46], but the relaxation rate σ_{TF} from a Gaussian fit is often used as an estimate of $\gamma_\mu \Delta B_{rms}$, where $\Delta B_{rms} = \langle \Delta B^2 \rangle^{1/2}$ is the rms width of the field distribution in the vortex lattice. For H_{TF} close to H_{c1}, Brandt [47] showed that

$$\langle \Delta B^2 \rangle = 0.00371 \, \Phi_0^2 / \Lambda^4 \qquad (2)$$

in the London limit $\Lambda \gg$ coherence length ξ, where Λ is the London penetration depth and Φ_0 is the flux quantum. In turn, from the London equations, Λ is related to the superfluid density ρ_s and the carrier effective mass m_{eff} by

$$\frac{1}{\Lambda^2} = \frac{4\pi e^2 \rho_s}{m_{eff} c^2}. \qquad (3)$$

Thus, $\rho_s \propto \sigma_{TF}$.

Figure 6 gives the temperature dependencies of the TF relaxation rates from fits of Eq. (A7) to the data. The zero-temperature superfluid density $\rho_s(0)$ from $\sigma_{TF}(T \to 0)$ varies somewhat with x but is remarkably insensitive to Nd doping up to $x = 0.20$, where T_c has decreased by more than 20% (Fig. 1).

In principle, the temperature dependence of σ_{TF} and hence of ρ_s yields information on the symmetry of the superconducting energy gap. In PrOs$_4$Sb$_{12}$, $\rho_s(0) \approx 10^{22}$ cm^{-3} [4], or

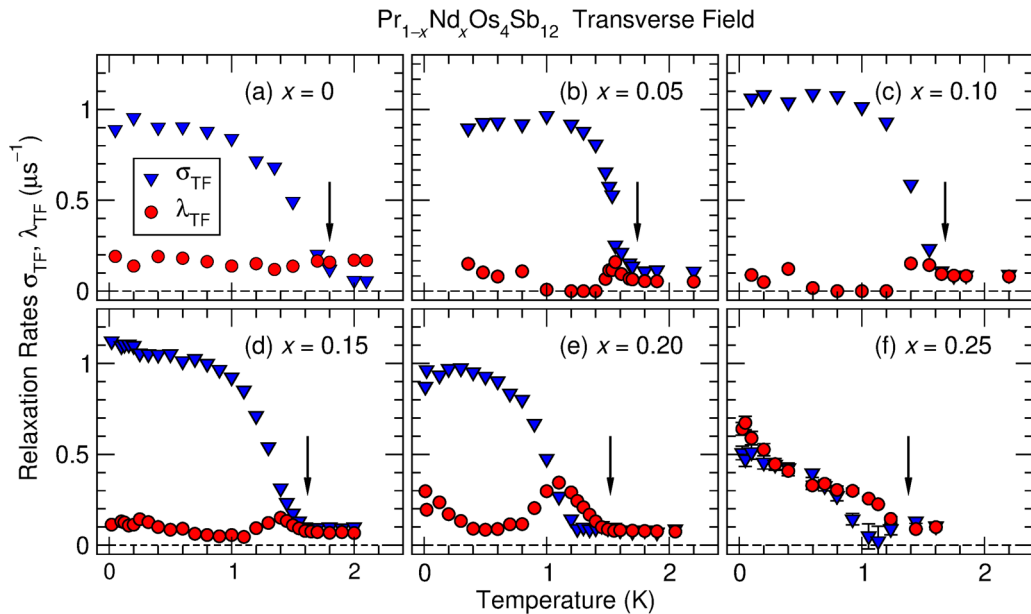FIG. 6. Temperature dependence of transverse-field relaxation rates σ_{TF} and λ_{TF} in $Pr_{1-x}Nd_xOs_4Sb_{12}$ from fits of Eq. (A7) to the data. Transverse magnetic field $H_{TF} = 200$ Oe for $x = 0$, 100 Oe for $x > 0$. Triangles: Gaussian relaxation rate σ_{TF}. Circles: Exponential damping rate λ_{TF}. Arrows: Superconducting transition temperatures T_c.

roughly eight carriers per cubic unit cell. This is somewhat high compared to band-theoretical Fermi volumes [48], but no more than order-of-magnitude agreement can be expected given the approximations in the μSR analysis. Moreover, the temperature dependence of σ_{TF} is consistent with the absence of superconducting gap nodes [4,8,9], whereas Meissner-state rf penetration-depth measurements [6] were taken as evidence for point nodes. This difference can be accounted for by a second smaller gap, which contributes to the Meissner state $\Lambda(T)$ but not significantly to the vortex-state field distribution [8,9]. Multiband superconductivity has been observed in $PrOs_4Sb_{12}$ by other techniques [3,49,50]. Multiple gaps complicate analysis of the temperature dependence of ρ_s [51].

A significant difficulty with the present data is the statistical anticorrelation between σ_{TF} and λ_{TF} in Eq. (A7), an effect that was noted previously [9] and discussed above in Sec. IV A for ZF μSR fits. The correlation coefficient magnitudes for these parameters in Eq. (A7) are large, $\sim$0.8. For $x = 0$, $\lambda_{TF}(T)$ is essentially constant [Fig. 6(a)] and was fixed at its normal-state value in previous analyses [8,9]. This cannot be done for $x > 0$, since $\lambda_{TF}(T)$ exhibits significant temperature dependence [Figs. 6(b)–6(f)]. The data behave unevenly across the alloy series, and σ_{TF}-λ_{TF} anticorrelation is suggested, particularly at low temperatures. Thus, determining the penetration depth from $\sigma_{TF}(T, x > 0)$ is problematic.

2. Exponential rate

For $x = 0$, the TF exponential damping rate $\lambda_{TF}(T)$ [Fig. 6(a)] is nearly temperature independent, as noted above and previously reported [4,11,44] (and approximately the same as the ZF rate, cf. Fig. 5).

But $\lambda_{TF}(T)$ acquires considerable structure in the alloys [Figs. 6(b)–6(f)]. The two main features are increases with decreasing temperature at low temperatures and peaks below T_c

(which are shown by arrows in Fig. 6). Both of these anomalies increase with Nd concentration. The low-temperature increase of $\lambda_{TF}(T)$ is consistent with that observed in the ZF dynamic rate $\lambda_d(T)$ and discussed in Sec. IV A.

The peaks are reminiscent of the coherence peak due to conduction-electron spin-lattice (dynamic) nuclear relaxation in a fully gapped superconductor [52]. Alternatively, a peak at a magnetic transition would be expected from critical slowing down of dynamic spin fluctuations at the transition. But both of these phenomena involve dynamic relaxation, so peaks should also be observed in ZF $\lambda_d(T)$. This is not the case (Fig. 5), and therefore dynamic relaxation is unlikely. Furthermore, there is no evidence for a magnetic transition near T_c.

We speculate that the peaks are due to the onset of Lorentzian-like distributions of static local fields at T_c [53], which narrow at low temperatures. Two candidate mechanisms for this are (i) impurity-assisted flux pinning and (ii) inhomogeneity in T_c. Both would disappear at low temperatures; the former when the applied field is well below H_{c2}, and the latter when the entire sample volume is superconducting. More work is clearly needed to understand this feature of the data.

V. CONCLUSIONS

We have carried out a study of Pr-rich $Pr_{1-x}Nd_xOs_4Sb_{12}$ alloys ($0 \leqslant x \leqslant 0.25$) using the μSR technique. A spontaneous internal field, found below the superconducting T_c in the end compound $x = 0$ and attributed to broken TRS [11,31], is not observed for $x \geqslant 0.05$. It is surprisingly indicating that the magnetic substitution of Nd for Pr suppresses broken TRS rapidly. At higher Nd concentrations, the dynamic relaxation rate λ_d increases with decreasing temperature as $T \to 0$ (Fig. 5), suggestive of critical slowing as a magnetic phase transition is approached. There is, however, no sign of static

magnetism or magnetic moment freezing of Nd^{3+} down to the lowest temperatures of measurement.

The $T = 0$ superfluid density $\rho_s(0, x)$ from TF μSR measurements of σ_{TF} (Fig. 6) is remarkably independent of x up to ~ 0.2, even though the suppression of T_c has reached more than 20% of $PrOs_4Sb_{12}$'s (Fig. 1). The expected behavior of $\rho_s(0, x)$ in the presence of multiple gaps and magnetic impurities is complex [51], but the weak impurity concentration dependence is evidence that neither the restoration of TRS nor the initial suppression of T_c is accompanied by a major change in the superconducting state.

All the above are unexpected phenomena discovered in the current study. Further investigation is needed to understand the enigmatic behavior of $Pr_{1-x}Nd_xOs_4Sb_{12}$.

ACKNOWLEDGMENTS

APPENDIX: DATA ANALYSIS

Here we summarize the μSR analysis procedures used in the present paper. Comprehensive reviews of the μSR technique are cited in Ref. [10].

In a typical μSR experiment, 100% spin-polarized positive muons (μ^+) are implanted and stop at interstitial sites in the sample. Each muon decays according to the reaction $\mu^+ \rightarrow e^+ + \nu_e + \overline{\nu}_\mu$, with a lifetime $\tau_\mu \approx 2.197 \,\mu$s. The decay positron is emitted preferentially in the direction of the μ^+ spin at the time of decay. Individual positrons are detected using an array of scintillation counters surrounding the sample. A positron event in the ith counter at time t after the corresponding μ^+ implantation increments the histogram bin $N_i(t)$ for this time by 1.

The resulting histogram is given by

$$N_i(t) = N_i^0 e^{-t/\tau_\mu}[1 + A_i G_i(t)], \quad (A1)$$

where $G_i(t)$ is the time evolution of the μ^+ ensemble spin polarization component in the direction of the counter [$G_i(t=0)$ is normalized to 1 for 100% spin polarization], $N_i^0(1 + A_i)$ is the initial count rate, and A_i is the initial count asymmetry, spectrometer dependent but usually ~ 0.2–0.25 [10]. Thus the experiment measures $G_i(t)$, which contains information on local static and dynamic magnetic fields at μ^+ sites in the sample.

For two identical counters 1 and 2 on opposite sides of the sample ($N_2^0 = N_1^0$, $A_2 = -A_1$), the asymmetry time spectrum $A(t)$ is given by

$$A(t) = \frac{N_1(t) - N_2(t)}{N_1(t) + N_2(t)} = A_1 G(t). \quad (A2)$$

In practice, the two counters and their environments are seldom identical, but differences can be measured in calibration experiments and accounted for in data analysis [54].

In longitudinal-field (LF) μSR [55] and ZF μSR (a special case of LF μSR) the counters and magnetic field, if any, are aligned parallel to the initial μ^+ polarization. In a TF μSR experiment the counters and initial μ^+ spin polarization are aligned perpendicular to the field.

A spurious signal is often present due to muons that miss the sample and stop in the sample holder. This is usually made of silver, which in addition to good thermal conductivity exhibits a simple μSR signal due to weak nuclear magnetism. In that case,

$$G(t) = (1 - f_{Ag})G_{samp}(t) + f_{Ag}G_{Ag}(t), \quad (A3)$$

where G_{samp} and G_{Ag} are the μ^+ spin polarizations of the sample and silver, respectively, and f_{Ag} is the fraction of muons that stop in the sample holder. In the present experiments, f_{Ag} varied with sample size and mounting in the range 0.3–0.4. ZF μ^+ spin relaxation in silver is slow on the time scale of the sample relaxation (rate $\sim 0.015 \,\mu s^{-1}$). This has been included in $G_{Ag}(t)$, but it does not affect the results appreciably.

Fits to the data can be made either to separate histograms [Eq. (A1)] or to the asymmetry time spectrum [Eq. (A2)]. The fit parameters are the A_i, parameters that define $G_{samp}(t)$ (relaxation rates, frequencies, etc.), f_{Ag}, and other spectrometer-dependent parameters. The procedure can be applied to either LF/ZF μSR or TF μSR data.

For simplicity, $G_{samp}(t)$ is referred to as $G(t)$ in the following and the main text.

1. Zero field

a. Static relaxation. In ZF, the relaxation function $G(t)$ is extremely sensitive to the behavior of the local magnetic field $\mathbf{B}_{loc}$ at μ^+ sites, since there is no competing applied field. If dynamic relaxation is negligible, μ^+ precession in $\mathbf{B}_{loc}$ results in static relaxation of $G(t)$ if the magnitude B_{loc} is distributed. The spin component of each muon parallel to $\mathbf{B}_{loc}$ does not precess, however, leading to a constant term in $G(t)$ [37]. If $\mathbf{B}_{loc}$ is randomly oriented, in zero applied field the component of nonprecessing μ^+ polarization in the initial polarization direction is 1/3 the initial polarization [10], so $G(t)$ relaxes from 1 at $t = 0$ to 1/3 at late times.

In the static Gaussian KT model [37], the distribution of static field components is modeled by a Gaussian of width Δ_{KT}/γ_μ and zero mean. In ZF, the static KT μ^+ spin relaxation function resulting from this field distribution is

$$G_G(\Delta_{KT}, t) = \tfrac{1}{3} + \tfrac{2}{3}[1 - (\Delta_{KT}t)^2] \exp\left[-\tfrac{1}{2}(\Delta_{KT}t)^2\right]. \quad (A4)$$

This model is applicable when $\mathbf{B}_{loc}$ is the sum of randomly oriented quasistatic nuclear dipolar fields at μ^+ sites if, as is often the case, nuclear moment fluctuations are slow on the muon timescale [37]. The dipole field distribution is approximately Gaussian because random fields from several nuclei contribute and the central limit theorem is approximately valid.

Equation (A4) also models the effect of additional static contributions to $\mathbf{B}_{loc}$ if their distribution is approximately

Gaussian (e.g., the spontaneous fields observed below T_c in $PrOs_4Sb_{12}$ [11]).

A convolution of static Gaussian and Lorentzian field distributions yields the ZF static Voigtian KT relaxation function [38]

$$G_V(\Delta_{KT}, a, t) = \tfrac{1}{3} + \tfrac{2}{3}[1 - at - (\Delta_{KT}t)^2]$$
$$\times \exp\left[-at - \tfrac{1}{2}(\Delta_{KT}t)^2\right], \quad (A5)$$

where a/γ_μ is the half width of the Lorentzian distribution. Exponentially damped Voigtian KT relaxation [Eq. (A6) with $G_{stat}(t) = G_V(\Delta_{KT}, a, t)$] has been observed in the filled skutterudite superconductor $PrPt_4Ge_{12}$ [56], and is therefore a candidate for describing the present experimental results. However, damped Voigtian KT fits to the present data yield exponential Voigtian rate $a \approx 0$, which are therefore equivalent to damped Gaussian KT fits. As discussed in Sec. III A, there is no evidence for a Lorentzian component to the static field distribution.

b. Dynamic Relaxation. Dynamic μ^+ spin relaxation ("spin-lattice" relaxation in the NMR literature) is due to thermally-fluctuating components of $\mathbf{B}_{loc}$, which induce transitions between μ^+ spin states and relax $G(t)$ to its thermal equilibrium value (essentially zero in μSR). A damping factor $\exp(-\lambda_d t)$ is often used to model dynamic relaxation in the presence of static relaxation:

$$G(t) = e^{-\lambda_d t} G_{stat}(t), \quad (A6)$$

where $G_{stat}(t)$ is the appropriate static relaxation function [i.e., Eq. (A4) or (A5)]. The exponential form of the damping assumes that the fluctuating field at each μ^+ site results in the same dynamic relaxation rate, even though the static local fields are distributed, and that the fluctuation rate is rapid compared to the rms amplitude of the fluctuating field; this is the so-called motionally narrowed limit.

2. Transverse field

In TF, μSR $G(t)$ is dominated by μ^+ precession in the applied field. In the presence of both exponential and Gaussian contributions to the damping, data are often fit by the TF relaxation function

$$G_{TF}(t) = \exp\left[-\lambda_{TF}t - \tfrac{1}{2}(\sigma_{TF}t)^2\right]\cos(\omega t + \phi) \quad (A7)$$

for applied transverse field $H_{TF} \gg B_{loc}$, where $\omega = \gamma_\mu H_{TF}$, σ_{TF}/γ_μ is the width of the Gaussian field distribution and ϕ is the phase of the oscillation, determined by the geometry of the spectrometer. Whether the exponential TF rate λ_{TF} in Eq. (A7) is static or dynamic in origin cannot be determined from TF μSR alone.

---

[1] E. D. Bauer, N. A. Frederick, P.-C. Ho, V. S. Zapf, and M. B. Maple, Superconductivity and heavy fermion behavior in $PrOs_4Sb_{12}$, Phys. Rev. B **65**, 100506(R) (2002).

[2] E. A. Goremychkin, R. Osborn, E. D. Bauer, M. B. Maple, N. A. Frederick, W. M. Yuhasz, F. M. Woodward, and J. W. Lynn, Crystal Field Potential of $PrOs_4Sb_{12}$: Consequences for Superconductivity, Phys. Rev. Lett. **93**, 157003 (2004).

[3] G. Seyfarth, J. P. Brison, M.-A. Méasson, J. Flouquet, K. Izawa, Y. Matsuda, H. Sugawara, and H. Sato, Multiband Superconductivity in the Heavy Fermion Compound $PrOs_4Sb_{12}$, Phys. Rev. Lett. **95**, 107004 (2005).

[4] D. E. MacLaughlin, J. E. Sonier, R. H. Heffner, O. O. Bernal, B.-L. Young, M. S. Rose, G. D. Morris, E. D. Bauer, T. D. Do, and M. B. Maple, Muon Spin Relaxation and Isotropic Pairing in Superconducting $PrOs_4Sb_{12}$, Phys. Rev. Lett. **89**, 157001 (2002).

[5] K. Izawa, Y. Nakajima, J. Goryo, Y. Matsuda, S. Osaki, H. Sugawara, H. Sato, P. Thalmeier, and K. Maki, Multiple Superconducting Phases in New Heavy Fermion Superconductor $PrOs_4Sb_{12}$, Phys. Rev. Lett. **90**, 117001 (2003).

[6] E. E. M. Chia, M. B. Salamon, H. Sugawara, and H. Sato, Probing the Superconducting Gap Symmetry of $PrOs_4Sb_{12}$: A Penetration Depth Study, Phys. Rev. Lett. **91**, 247003 (2003).

[7] K. Grube, S. Drobnik, C. Pfleiderer, H. v. Löhneysen, E. D. Bauer, and M. B. Maple, Specific heat and ac susceptibility studies of the superconducting phase diagram of $PrOs_4Sb_{12}$, Phys. Rev. B **73**, 104503 (2006).

[8] D. E. MacLaughlin, L. Shu, R. H. Heffner, J. E. Sonier, F. D. Callaghan, G. D. Morris, O. O. Bernal, W. M. Yuhasz, N. A. Frederick, and M. B. Maple, Multiband superconductivity and penetration depth in $PrOs_4Sb_{12}$, Phys. B: Condens. Matter **403**, 1132 (2008).

[9] L. Shu, D. E. MacLaughlin, W. P. Beyermann, R. H. Heffner, G. D. Morris, O. O. Bernal, F. D. Callaghan, J. E. Sonier, W. M. Yuhasz, N. A. Frederick, and M. B. Maple, Penetration depth, multiband superconductivity, and absence of muon-induced perturbation in superconducting $PrOs_4Sb_{12}$, Phys. Rev. B **79**, 174511 (2009).

[10] A. Schenck, *Muon Spin Rotation Spectroscopy: Principles and Applications in Solid State Physics* (A. Hilger, Bristol and Boston, 1985); J. H. Brewer, Muon spin rotation/relaxation/ resonance, in *Encyclopedia of Applied Physics*, edited by G. L. Trigg, E. S. Vera, and W. Greulich (VCH Publishers, New York, 1994), Vol. 11, pp. 23–53; J. H. Brewer, in *Encyclopedia of Applied Physics*, edited by G. L. Trigg, E. S. Vera, and W. Greulich (Wiley-VCH, Weinheim, 2003); S. J. Blundell, Spin-polarized muons in condensed matter physics, Contemp. Phys. **40**, 175 (1999); *Muon Science: Muons in Physics, Chemistry and Materials*, edited by S. L. Lee, S. H. Kilcoyne, and R. Cywinski, Scottish Universities Summer School in Physics Vol. 51 (Institute of Physics Publishing, Bristol and Philadelphia, 1999); A. Yaouanc and P. Dalmas de Réotier, *Muon Spin Rotation, Relaxation, and Resonance: Applications to Condensed Matter*, International Series of Monographs on Physics (Oxford University Press, New York, 2011).

[11] Y. Aoki, A. Tsuchiya, T. Kanayama, S. R. Saha, H. Sugawara, H. Sato, W. Higemoto, A. Koda, K. Ohishi, K. Nishiyama, and R. Kadono, Time-Reversal Symmetry-Breaking Superconductivity in Heavy-Fermion $PrOs_4Sb_{12}$ Detected by Muon-Spin Relaxation, Phys. Rev. Lett. **91**, 067003 (2003).

[12] S. K. Ghosh, M. Smidman, T. Shang, J. F. Annett, A. D. Hillier, J. Quintanilla, and H. Yuan, Recent progress on superconductors with time-reversal symmetry breaking, J. Phys.: Condens. Matter **33**, 033001 (2021).

[13] P.-C. Ho, N. A. Frederick, V. S. Zapf, E. D. Bauer, T. D. Do, M. B. Maple, A. D. Christianson, and A. H. Lacerda, High-field ordered and superconducting phases of the heavy fermion compound $PrOs_4Sb_{12}$, Phys. Rev. B **67**, 180508(R) (2003).

[14] M. Kohgi, K. Iwasa, M. Nakajima, N. Metok, S. Araki, N. Bernhoeft, J.-M. Mignot, A. Gukasov, H. Sato, Y. Aoki, and H. Sugawara, Evidence for magnetic-field-induced quadrupolar ordering in the heavy-fermion superconductor $PrOs_4Sb_{12}$, J. Phys. Soc. Jpn. **72**, 1002 (2003).

[15] K. Miyake, H. Kohno, and H. Harima, Theory of a new type of heavy-electron superconductivity in $PrOs_4Sb_{12}$: Quadrupolar-fluctuation mediated odd-parity pairings, J. Phys.: Condens. Matter **15**, L275 (2003).

[16] M. Koga, M. Matsumoto, and H. Shiba, Roles of multipoles and excitons in superconductor $PrOs_4Sb_{12}$ With T_h Symmetry, J. Phys. Soc. Jpn. **75**, 014709 (2006).

[17] P. Thalmeier, Triplet superconductivity through quadrupolar exciton exchange in $PrOs_4Sb_{12}$, Phys. B: Condens. Matter **378-380**, 261 (2006).

[18] K. Katayama, S. Kawasaki, M. Nishiyama, H. Sugawara, D. Kikuchi, H. Sato, and G.-Q. Zheng, Evidence for point nodes in the superconducting gap function in the filled skutterudite heavy-fermion compound $PrOs_4Sb_{12}$: ^{123}Sb-NQR study under pressure, J. Phys. Soc. Jpn. **76**, 023701 (2007).

[19] H. Tou, Y. Inaoka, M. Doi, M. Sera, K. Asaki, H. Kotegawa, H. Sugawara, and H. Sato, Possible mass enhancement by multipole fluctuations excited via the singlet-triplet crystal electric field states in $PrOs_4Sb_{12}$: Sb-NMR studies using a single crystal, J. Phys. Soc. Jpn. **80**, 074703 (2011).

[20] E. D. Bauer, A. Ślebarski, E. J. Freeman, C. Sirvent, and M. B. Maple, Kondo insulating behaviour in the filled skutterudite compound $CeOs_4Sb_{12}$, J. Phys.: Condens. Matter **13**, 4495 (2001).

[21] M. Yogi, H. Kotegawa, G.-Q. Zheng, Y. Kitaoka, S. Ohsaki, H. Sugawara, and H. Sato, Novel phase transition near the quantum critical point in the filled skutterudite compound $CeOs_4Sb_{12}$: An Sb-NQR study, J. Phys. Soc. Jpn. **74**, 1950 (2005).

[22] C. Yang, Z. Zhou, H. Wang, J. Hu, K. Iwasa, H. Sugawara, and H. Sato, Evidence of spin density wave of $CeOs_4Sb_{12}$, Rare Metals **25**, 550 (2006).

[23] C. P. Yang, H. Wang, J. F. Hu, K. Iwasa, K. Kohgi, H. Sugawara, and H. Sato, Antiferromagnetic ordering of $CeOs_4Sb_{12}$ below 1K, J. Phys. Chem. C **111**, 2391 (2007).

[24] W. M. Yuhasz, N. A. Frederick, P.-C. Ho, N. P. Butch, B. J. Taylor, T. A. Sayles, M. B. Maple, J. B. Betts, A. H. Lacerda, P. Rogl, and G. Giester, Heavy fermion behavior, crystalline electric field effects, and weak ferromagnetism in $SmOs_4Sb_{12}$, Phys. Rev. B **71**, 104402 (2005).

[25] P.-C. Ho, W. M. Yuhasz, N. P. Butch, N. A. Frederick, T. A. Sayles, J. R. Jeffries, M. B. Maple, J. B. Betts, A. H. Lacerda, P. Rogl, and G. Giester, Ferromagnetism and possible heavy-fermion behavior in single crystals of $NdOs_4Sb_{12}$, Phys. Rev. B **72**, 094410 (2005).

[26] M. B. Maple, N. A. Frederick, P.-C. Ho, W. M. Yuhasz, and T. Yanagisawa, Unconventional superconductivity and heavy fermion behavior in $PrOs_4Sb_{12}$, J. Supercond. Novel Magn. **19**, 299 (2006).

[27] P.-C. Ho, T. Yanagisawa, N. P. Butch, W. M. Yuhasz, C. C. Robinson, A. A. Dooraghi, and M. B. Maple, A comparison of the normal and superconducting state properties of $Pr(Os_{1-x}Ru_x)_4Sb_{12}$ and $Pr_{1-x}Nd_xOs_4Sb_{12}$, Phys. B: Condens. Matter **403**, 1038 (2008).

[28] P.-C. Ho, T. Yanagisawa, W. M. Yuhasz, A. A. Dooraghi, C. C. Robinson, N. P. Butch, R. E. Baumbach, and M. B. Maple, Superconductivity, magnetic order, and quadrupolar order in the filled skutterudite system $Pr_{1-x}Nd_xOs_4Sb_{12}$, Phys. Rev. B **83**, 024511 (2011).

[29] D. E. MacLaughlin, P.-C. Ho, L. Shu, O. O. Bernal, S. Zhao, A. A. Dooraghi, T. Yanagisawa, M. B. Maple, and R. H. Fukuda, Muon spin rotation and relaxation in $Pr_{1-x}Nd_xOs_4Sb_{12}$: Magnetic and superconducting ground states, Phys. Rev. B **89**, 144419 (2014).

[30] Y. Aoki, T. Tayama, T. Sakakibara, K. Kuwahara, K. Iwasa, M. Kohgi, W. Higemoto, D. E. MacLaughlin, H. Sugawara, and H. Sato, The unconventional superconductivity of skutterudite $PrOs_4Sb_{12}$: Time-reversal symmetry breaking and adjacent field-induced quadrupole ordering, J. Phys. Soc. Jpn. **76**, 051006 (2007).

[31] L. Shu, W. Higemoto, Y. Aoki, A. D. Hillier, K. Ohishi, K. Ishida, R. Kadono, A. Koda, O. O. Bernal, D. E. MacLaughlin, Y. Tunashima, Y. Yonezawa, S. Sanada, D. Kikuchi, H. Sato, H. Sugawara, T. U. Ito, and M. B. Maple, Suppression of time-reversal symmetry breaking superconductivity in $Pr(Os_{1-x}Ru_x)_4Sb_{12}$ and $Pr_{1-y}La_yOs_4Sb_{12}$, Phys. Rev. B **83**, 100504(R) (2011).

[32] J. E. Crow and R. D. Parks, The transition temperature of superconductors with paramagnetic impurities, Phys. Lett. **21**, 378 (1966).

[33] J. L. Smith, Z. Fisk, J. O. Willis, H. R. Ott, S. E. Lambert, Y. Dalichaouch, and M. B. Maple, Impurities in UBe_{13}, J. Magn. Magn. Mater. **63-64**, 464 (1987).

[34] Applied magnetic field perpendicular to the initial muon spin direction.

[35] W. Jeitschko and D. Braun, $LaFe_4P_{12}$ with filled $CoAs_3$-type structure and Isotypic lanthanoid-transition metal polyphosphides, Acta Cryst. B **33**, 3401 (1977).

[36] A. Suter and B. Wojek, Musrfit: A free platform-independent framework for μSR data analysis, Phys. Procedia **30**, 69 (2012).

[37] R. Kubo and T. Toyabe, A stochastic model for low field resonance and relaxation, in *Magnetic Resonance and Relaxation*, edited by R. Blinc (North-Holland, Amsterdam, 1967), pp. 810–823; R. S. Hayano, Y. J. Uemura, J. Imazato, N. Nishida, T. Yamazaki, and R. Kubo, Zero- and low-field spin relaxation studied by positive muons, Phys. Rev. B **20**, 850 (1979).

[38] M. R. Crook and R. Cywinski, Voigtian Kubo-Toyabe muon spin relaxation, J. Phys.: Condens. Matter **9**, 1149 (1997).

[39] A. Balatsky, Spontaneous time reversal and parity breaking in a d_{x2-y2}-WAVE superconductor with magnetic impurities, J. Phys. Chem. Solids **59**, 1689 (1998).

[40] M. E. Simon and C. M. Varma, Magnetic impurities in d-wave superconductors, Phys. Rev. B **60**, 9744 (1999).

[41] M. J. Graf, A. V. Balatsky, and J. A. Sauls, Local time-reversal-symmetry breaking in $d_{x^2-y^2}$ superconductors, Phys. Rev. B **61**, 3255 (2000).

[42] M. Sigrist and K. Ueda, Phenomenological theory of unconventional superconductivity, Rev. Mod. Phys. **63**, 239 (1991).

[43] T. Ohmi and K. Machida, Nonunitary Superconducting State in UPt$_3$, Phys. Rev. Lett. **71**, 625 (1993).

[44] L. Shu, D. E. MacLaughlin, Y. Aoki, Y. Tunashima, Y. Yonezawa, S. Sanada, D. Kikuchi, H. Sato, R. H. Heffner, W. Higemoto, K. Ohishi, T. U. Ito, O. O. Bernal, A. D. Hillier, R. Kadono, A. Koda, K. Ishida, H. Sugawara, N. A. Frederick, W. M. Yuhasz *et al.*, Muon spin relaxation and hyperfine-enhanced ^{141}Pr nuclear spin dynamics in Pr(Os,Ru)$_4$Sb$_{12}$ and (Pr,La)Os$_4$Sb$_{12}$, Phys. Rev. B **76**, 014527 (2007).

[45] J. E. Sonier, J. H. Brewer, and R. F. Kiefl, μSR studies of the vortex state in type-II superconductors, Rev. Mod. Phys. **72**, 769 (2000).

[46] J. E. Sonier, Muon spin rotation studies of electronic excitations and magnetism in the vortex cores of superconductors, Rep. Prog. Phys. **70**, 1717 (2007).

[47] E. H. Brandt, Flux distribution and penetration depth measured by muon spin rotation in high-T_c superconductors, Phys. Rev. B **37**, 2349 (1988).

[48] H. Sugawara, S. Osaki, S. R. Saha, Y. Aoki, H. Sato, Y. Inada, H. Shishido, R. Settai, Y. Ōnuki, H. Harima, and K. Oikawa, Fermi surface of the heavy-fermion superconductor PrOs$_4$Sb$_{12}$, Phys. Rev. B **66**, 220504(R) (2002).

[49] M.-A. Méasson, D. Braithwaite, J. Flouquet, G. Seyfarth, J. P. Brison, E. Lhotel, C. Paulsen, H. Sugawara, and H. Sato, Superconducting phase diagram of the filled skutterudite PrOs$_4$Sb$_{12}$, Phys. Rev. B **70**, 064516 (2004).

[50] J. Juraszek, R. Wawryk, Z. Henkie, M. Konczykowski, and T. Cichorek, Symmetry of Order Parameters in Multiband Superconductors LaRu$_4$As$_{12}$ and PrOs$_4$Sb$_{12}$ Probed by Local Magnetization Measurements, Phys. Rev. Lett. **124**, 027001 (2020).

[51] R. Prozorov and R. W. Giannetta, Magnetic penetration depth in unconventional superconductors, Supercond. Sci. Technol. **19**, R41 (2006); V. G. Kogan, R. Prozorov, and V. Mishra, London penetration depth and pair breaking, Phys. Rev. B **88**, 224508 (2013).

[52] L. C. Hebel and C. P. Slichter, Nuclear spin relaxation in normal and superconducting aluminum, Phys. Rev. **113**, 1504 (1959).

[53] A Lorentzian distribution of static fields results in exponential muon spin relaxation [10].

[54] T. M. Riseman, J. H. Brewer, and D. J. Arseneau, Corrected asymmetry plots, Hyperfine Interact. **87**, 1135 (1994).

[55] Not used in the present experiments.

[56] A. Maisuradze, W. Schnelle, R. Khasanov, R. Gumeniuk, M. Nicklas, H. Rosner, A. Leithe-Jasper, Y. Grin, A. Amato, and P. Thalmeier, Evidence for time-reversal symmetry breaking in superconducting PrPt$_4$Ge$_{12}$, Phys. Rev. B **82**, 024524 (2010).